Recent Progress on Achromatic Metalenses

**Qikai Chen[1], Yitian Liu[1], Yaoyuan Lei[1],
Sijie Pian[1], Zhuning Wang[1], and Yaoguang Ma[1, 2, *]**

(*Invited Review*)

Abstract—As a potential alternative to conventional lenses, metalenses have the advantage of ultrathin volume and light weight over conventional lenses. Such miniaturization is expected to apply to compact, nanoscale optical devices such as micro-cameras and high-resolution display. However, chromatic aberration is an important problem in the practical application of metalenses, which will damage the imaging resolution and color reality for multi-wavelength incident light. Here, we briefly discuss recent development of design methods for achromatic metalenses, containing one or more pieces, and experimental evaluation of their performances.

1. INTRODUCTION

Metasurfaces are special structures consisting of subwavelength scale unit cells, which can modulate phase, amplitude, polarization, and angular momentum of incident light. By changing the geometry parameters or materials of the atoms [1] with designed spatial distribution, one can shape the wavefront of outputting light at will. The high spatial resolution modulation enables metasurfaces with a higher degree of design freedom. Thus they have been widely investigated as optical components or devices, such as lenses [2–6], gratings [3, 4], holograms [7], and spectrometers [8–10], showing great application potential. The light weight and ultrathin thickness of metasurfaces offer an opportunity to reduce bulky volume of conventional refractive lenses. Therefore, metalenses can act as lenses in compact devices. However, they still face lots of challenges before being put into practical use, even fitting the lens phase with meta-atoms accurately.

The design of single-wavelength metalenses usually starts from the hyperbolic phase profile $\varphi(r)$ presented in Eq. (1) [2].

$$\varphi(r, \lambda) = -\frac{2\pi}{\lambda}\left(\sqrt{r^2 + f^2} - f\right) \tag{1}$$

where $r = \sqrt{(x^2 + y^2)}$ is the radial coordinate on the metalens, f the focal length, and λ the wavelength of normal incident light. With meta-atoms with proper phase shift to fit the phase profile digitally, the incident light can be focused by metalens. Mathematically, the phase profile can be folded within 2π, so the phase shifts provided by the meta-atoms only need to cover the 2π range. However, this discretization process by dividing the continuous phase profile to periods of meta-atoms results in a certain deviation between the real wavefront and ideal converging wave. In order to characterize the influence of discrete phase shift, Aieta et al. [11] designed a metalens and calculated the Strehl ratio under different phase gradients. Fig. 1 shows that when the number of phase levels is more than 4,
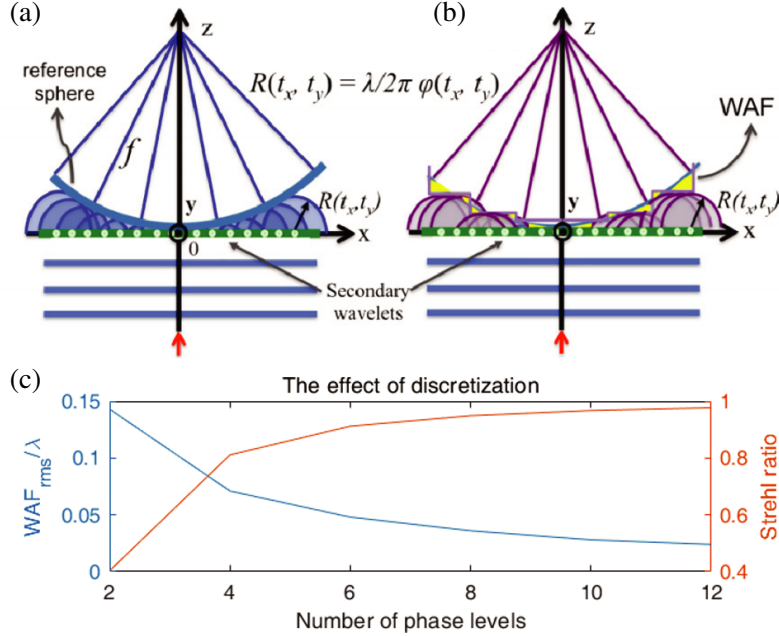
Figure 1. (a) The wavefront scattered by a metalens. For a very dense distribution of antennas, the phase function $\varphi(x, y)$ can be assumed continuous leading to a perfect spherical wavefront. (b) If the metalens is designed using a limited set of phase elements, the continuous phase function is replaced with a discrete distribution that introduces aberrations (the yellow region corresponds to the wave aberration function (WAF)). (c) The effect of the discretization of the phase function is evaluated by calculating the root mean square of the wave aberration function (WAF_{rms}) and the Strehl ratio for an increasing number of phase levels [11].

which means that incremental phase between adjacent atoms is less than $\pi/2$, the difference between the focusing effect of metalens and the airy disk becomes negligible (Strehl ratio > 0.8). However, it can be derived from Eq. (1) that the phase gradient will increase while the required radius becomes larger, so metalenses face a phase fitting problem in large aperture design.

As for imaging systems, the result will significantly influenced by the strong dispersion of metalenses. Therefore, chromatic aberration introduces different phase profiles at different wavelengths and should be corrected in the design process. To achieve achromatic focusing, researches have tried to find meta-atoms to fit all phase profiles simultaneously by considering different kinds of unique structure, optimizing the arrangement of atoms, improving optimization methods, and involving atoms' field coupling. Besides, time-bandwidth product constraint should be considered who will limit the aperture size of achromatic metalenses. In this paper, we review recent progress on the design methods of achromatic metalenses, summarize the merit and demerit, and compare their notable performances. The design parameters and characteristics are listed in Table 1 and Table 2.

2. DESIGN METHODS OF ACHROMATIC METALENSES

According to the number of lenses or material layers used, we classify the achromatic metalenses into two cases: single lens and cascaded lenses.

2.1. Single-Piece Achromatic Metalenses

Because of the structural dispersion and material dispersion, a given atom responds differently to different wavelengths. When the geometric parameters of atoms change, the dispersion also changes. On the other hand, the hyperbolic phase profile should be satisfied under different wavelengths simultaneously, which may be out of the range of selectable atoms' dispersion and cause mismatch

Table 1. Single piece achromatic metalenses (Focusing efficiency is average value unless otherwise specified).

Method	Aperture (μm)	NA	Bandwidth (nm)	Characteristic	Focusing efficiency
Arbabi et al. [13] (Spatial multiplexing)	300	0.46	915, 1550	Transmission	10%, 58%
Khorasaninejad et al. [16] (Extra phase shift)	200	0.2	490–550	Reflection	15%
Arbabi et al. [17] (Extra phase shift)	500	0.28	1450–1590	Reflection	NA
Wang et al. [18] (IRUE with Berry phase)	50	0.106	400–660	Transmission	40%
Chen et al. [22] (GD and GDD)	25	0.2	470–670	Transmission	20% at 500 nm
Arbabi et al. [25] (GD and GDD)	500	0.28	1450–1590	Reflection	50%
Fan et al. [26] (GD and n_{eff})	14	0.086	430–780	Transmission	47%
Wang et al. [27] (High aspect ratios)	25	0.24	650–1000	Transmission	77%
Shrestha et al. [28] (GD and phase range)	100	0.24	1200–1650	Transmission	50%
Ndao et al. [29] (GD and phase)	20	0.12	640–1200	Transmission Fishnet atoms	70%
Chung et al. [30] (Inverse design)	12.5	0.1	450–700	Transmission	65%
Li et al. [32] (GD folding)	2000	0.7	488, 532, 658	Transmission	11%, 12%, 10%

of phase profile. All of these requirements make the establishment of proper meta-atoms difficult and complicated, and effective methods should be taken to solve the problem.

Spatial multiplexing used in Fresnel lenses [12] can be transferred into the design of achromatic metalenses [13–15]. By interleaving different groups of meta-atoms to fit phase profiles respectively, researchers used different parts of metalenses to focus incident light at separate wavelengths. In this way, atoms aimed at different wavelengths can be regarded as a new big atom, which inevitably cause a low space utilization. As a result, it usually suffers a great loss in focusing efficiency. Arbabi et al. [13] confirmed this idea by designing a metalens at $\lambda = 915$ nm and 1550 nm (shown in Fig. 2(a)), with focusing efficiency of 10% at wavelength 915 nm and 58% at wavelength 1550 nm. It is notable that the broad waveband between the discrete designed wavelengths remains large chromatic aberration in this design. When the designed wavelengths are increased to narrow the waveband, the space utilization of each wavelength will accordingly decrease, so this method cannot be applied in broad continuous waveband. Consequently, a better method is considering all the wavelengths for a single atom of metalenses at the same time. In 2016, Khorasaninejad et al. [16]. designed an achromatic metalens over 60 nm bandwidth in the visible range by adding an extra phase shift in the phase profile as a new degree of freedom, and it worked in reflection mode with a focal-length standard deviation of 2.7 μm shown in Fig. 2(b). They found that the phase profile to achieve diffraction-limited focusing for collimated

Table 2. Multi-piece achromatic metalenses.

Method	Aperture (μm)	NA	Bandwidth (nm)	Characteristic	Focusing efficiency
Chen et al. [37] (Meta-corrector)	1500	0.075	470–700	Transmission ±45° atoms	35%
Zhou et al. [43] (Cascaded atoms)	500	0.42	1180, 1400, 1680	Transmission	5.1%, 12.8%, 22%
Yao et al. [44] (Double-layer material)	100	0.24	620–675	Transmission	22%
McClung et al. [45] (Bi-layer metalenses)	600	0.2	450–650	Transmission Annual areas	NA
Kim et al. [46] (Doublet)	300/700	0.33, 0.38, 0.47	445, 532, 660	Transmission FOV 60°	Normal 9.27%, 24.8%, 52.6%
Huang et al. [47] (Doublet)	5/8.6	0.61	470–650	Transmission FOV 60°	50%
Li et al. [48] (Doublet Abbe number)	19.5	0.26	400–700	Transmission	50%

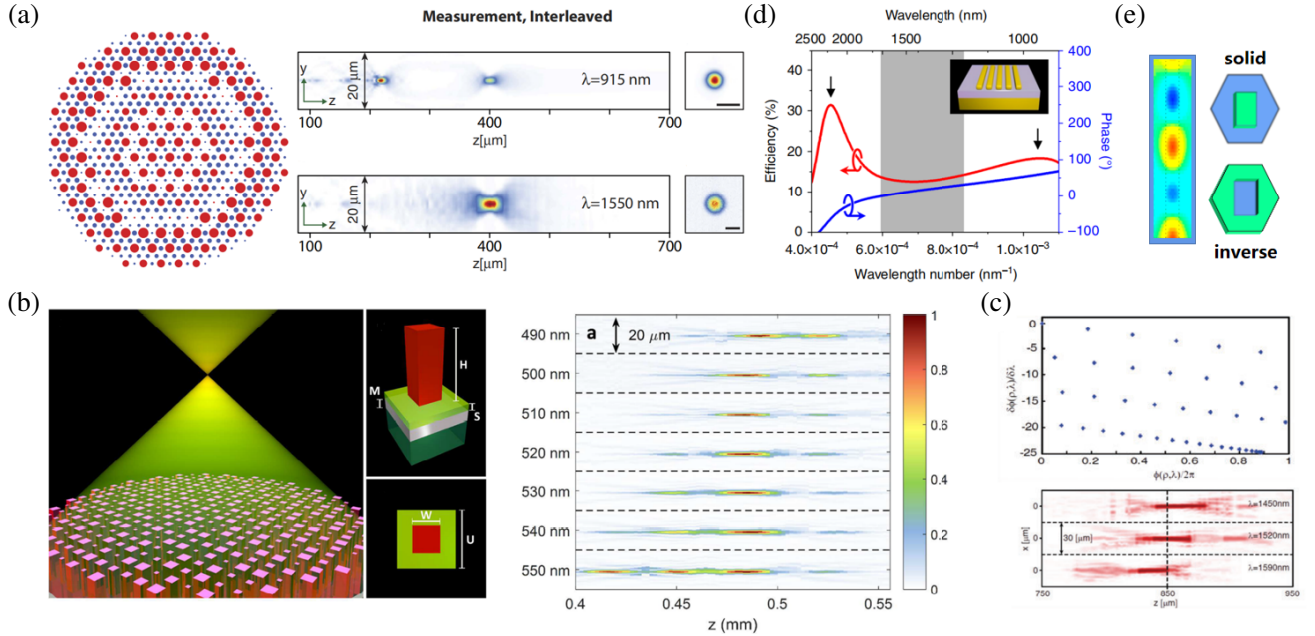**Figure 2.** (a) Double-wavelength metasurface lens formed by interleaving meta-atoms. Measured intensity profiles. Scale bars: 4 μm [13]. (b) Schematic of an AML achromatic metalens in reflection mode. Focal results at six different wavelength [16]. (c) Dispersion versus phase plot and measured results of metalens [17]. (d) IRUE. Gold atoms stand on a SiO$_2$/Au substrate. RCP-to-LCP polarization conversion efficiency [18]. (e) Schematic of waveguide-like IRUEs including solid and inverse nanostructures [21].

incident light can be written as

$$\varphi(r, \lambda) = C(\lambda) - \frac{2\pi}{\lambda}\left(\sqrt{r^2 + f^2} - f\right) \tag{2}$$

where $C(\lambda)$ is a reference phase whose value depends on the wavelength. This value offers an extra degree of freedom for multi-wavelength design, but has no influence on the focus effect of metalens. They chose the visible bandwidth from 490 to 550 nm and discretized it into six equally spaced wavelength, then determined the value of $C(\lambda)$ by utilizing the particle swarm optimization algorithm. By this way, they obtained an achromatic metalens in reflection mode with a focal-length standard deviation of 2.7 μm. In the same year, Arbabi et al. [17] proposed that dispersion $\partial\varphi/\partial\lambda$ should also be considered in the optimization process shown in Fig. 2(c). They demonstrated a dispersionless metalens from 1450 to 1590 nm at fifteen different wavelengths. Both methods require tons of atoms with different phase shifts at different wavelengths to fit all the phase profiles. As the design bandwidth increases, it becomes much more difficult to find proper atoms to satisfy all the requirements.

In 2017, Wang et al. [18] proposed a new way using integrated-resonant unit element (IRUE) for Berry phase based achromatic metalens design. For the design bandwidth ($\lambda_{\min} \sim \lambda_{\max}$), the equation of phase profile can be rewritten as

$$\varphi(r, \lambda) = \varphi(r, \lambda_{\max}) + \Delta\varphi(r, \lambda) \tag{3}$$

with

$$\Delta\varphi(r, \lambda) = -\left[2\pi\left(\sqrt{r^2 + f^2} - f\right)\right]\left(\frac{1}{\lambda} - \frac{1}{\lambda_{\max}}\right) \tag{4}$$

The $\varphi(r, \lambda_{\max})$ in Eq. (3) is considered as a basic profile independent of the wavelength λ and is acquired by Berry phase [19] of meta-atoms with different rotation angles. This idea has been widely used in achromatic researches with right-hand circular polarization (RCP) or left-hand circular polarization (LCP) incident light [20].

They found that the phase distribution between two plasmonic nano-rods resonances exhibits a smooth trend with a nearly linear profile against $1/\lambda$, and they named this phenomenon as IRUE shown in Fig. 2(d). Since this resonant phase response will not disturb Berry phase, it provides sufficient compensation for $\Delta\varphi$ in Eq. (3). Optimizing the total phase shifts, they demonstrated broadband achromatic metalenses over a continuous wavelength region from 1200 nm to 1680 nm with efficiency of around 12%. Wang et al. then applied this method in the visible region in 2018 [21], where they used solid and inverse IRUE consisted of GaN nanopillars and Al_2O_3 substrate working in transmission mode. Compared to plasmonic system, the induced optical fields are mostly concentrated inside the dielectric structures, so they acquired $1/\lambda$ phase compensation by waveguide-like cavity resonators shown in Fig. 2(e). The average efficiency of this metalens is about 40% over the 400 to 660 nm visible spectrum with focal length remaining almost unchanged.

In the same year, Chen et al. [22] explained the chromatic aberration by introducing the relative group delay (GD) and group delay dispersion (GDD) into the phase profile as shown in Fig. 3(a). They expanded Eq. (1) as a Taylor series near a design frequency ω_d as

$$\varphi(r, \lambda) = \varphi(r, \omega) = \varphi(r, \omega_d) + \left.\frac{\partial\varphi(r, \omega)}{\partial\omega}\right|_{\omega=\omega_d}(\omega - \omega_d) + \left.\frac{\partial^2\varphi(r, \omega)}{2\partial\omega^2}\right|_{\omega=\omega_d}(\omega - \omega_d)^2 + \cdots \tag{5}$$

Physically, the first term φ represents a spherical wavefront obtained by Berry phase. The second term $\partial\varphi/\partial\omega$ compensates for the difference of arrival times at focus for wavepackets passing through different regions of the metalens, which can be satisfied by GD of meta-atoms. The third and higher-order derivative terms represent GDD and higher dispersion order of wavepackets, and they ensure that the outgoing wavepackets are identical, which guarantees that the focus point will not be elongated. For metalens working in larger bandwidth, all the terms in the equation should be considered to minimize the time spread of wavepackets.

In their research, TiO_2 nanofins fabricated by electron-beam lithography (EBL) and atomic layer deposition (ALD) were used for the metalens design. Each unit consisted of one or more TiO_2 nanofins with varying dimensions. To better understand the design principle, these TiO_2 nanofins can also be treated as truncated waveguides [23], which introduce a phase shift for the transmitted light as

$$\varphi(r, \omega) = \frac{\omega}{c} n_{eff} h \tag{6}$$

where n_{eff} and h represent the effective index and the height of nanofins, respectively. As a result, the GD can be described as

$$\frac{\partial \varphi(r, \omega)}{\partial \omega} = \frac{h}{v_g} = \frac{1}{c} n_{eff} h + \frac{\omega}{c} \frac{\partial n_{eff}}{\partial \omega} h \tag{7}$$

Once the atoms' height and designed wavelength λ_d are determined ($\omega = \omega_d$), the GD mainly depends on nanofins' cross-section and material used. On the other hand, according to Eq. (1), the GD distribution on the metalens should obey the profile

$$\frac{\partial \varphi}{\partial \omega} = -\frac{1}{c} \left(\sqrt{r^2 + f^2} - f \right) \tag{8}$$

The GDD should be a constant if focal length f is not related with ω, which can be naturally compensated by the dispersion of truncated waveguides [24]. Satisfying all these phase and dispersion terms, they achieved a transmissive achromatic metalens from 470 nm to 670 nm with NA = 0.2, while the efficiency was about 20% at 500 nm.

However, these methods all take advantages of Berry phase, so the polarization of incident light must be LCP or RCP, which cannot be applied under linear incident light. Hence, Arbabi et al. [25] in 2017 demonstrated polarization insensitive meta-atoms with square cross-section in achromatic metalenses design shown in Fig. 3(b). They used silicon atoms on a SiO$_2$ and metal layer to construct zero dispersion metalens working in reflection mode over 1450 nm to 1590 nm. The reflection mode enables the obtained phase shifts to become larger by making light go through the atoms twice. However, satisfying dispersion requirement by such a simple structure of atoms remains a shortage of degrees of freedom. In 2019, Fan et al. [26] designed ten kinds of SiN atoms with four-fold symmetric cross section to solve this
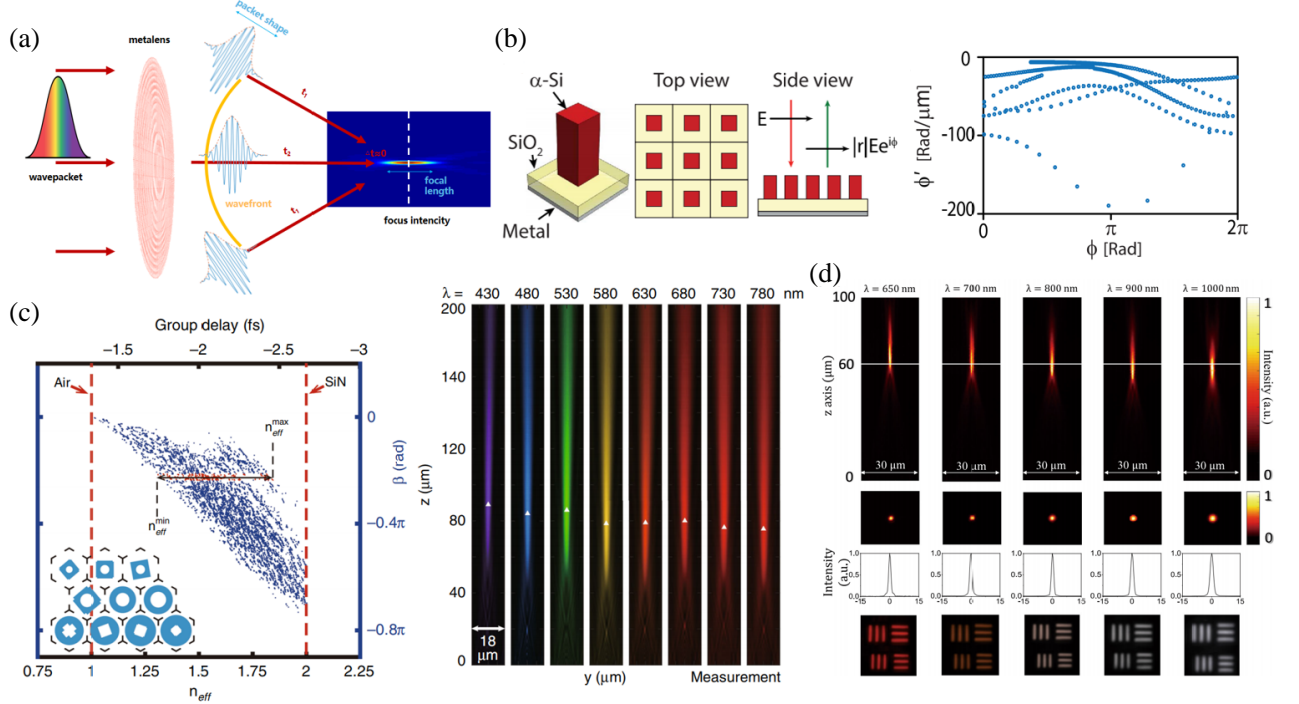

Figure 3. (a) Schematic of focusing process an achromatic metalens. Wavepackets from different locations arrive simultaneously at the focus. The yellow line shows the spherical wavefront. (b) Square amorphous silicon nano-post on a SiO$_2$ layer on a metallic reflector. Simulated dispersion-phase plot at λ_0 1520 nm [25]. (c) Calculated (n_{eff}, β) results for all considered SiN gratings. Blue points represent different gratings. Red dashed lines indicate the air and SiN materials. Measured normalized intensity distributions. The focal points are marked by white triangles [26]. (d) Intensity of focal spots in x-z plane and x-y planes at different wavelengths. The images of element-6, group-7 of the 1951 Unites States Air Force resolution [27].

problem. By this way, they increased the geometric freedom of atoms and guaranteed the polarization insensitive to incident light. In addition, they proposed a relationship between the maximum radius and effective refractive index. They combined Eq. (2) and Eq. (6) to obtain the relationship between n_{eff} and f as below

$$n_{eff}(r,\omega) = \frac{C(\omega)}{h} - \frac{1}{h}\left(\sqrt{r^2 + f^2} - f\right) \tag{9}$$

For a dispersionless metalens, which means $df/d\omega = 0$, Eq. (9) can be rewritten as

$$\frac{\partial n_{eff}(r,\omega)}{\partial \omega} = 0, \quad \omega \in [\omega_{\min}, \omega_{\max}] \tag{10}$$

That is to say, the achromatic bandwidth $\Delta\omega = \omega_{\max} - \omega_{\min}$ depends on the spectrum range sustained by the zero effective material dispersion. Furthermore, substituting Eq. (10) into Eq. (7), they acquired the relationship between n_{eff} and GD

$$n_{eff} = \frac{c}{h}\frac{\partial\varphi}{\partial\omega} \tag{11}$$

Therefore, the constraint between the effective refractive index and design aperture can be obtained from Eq. (8). For the whole metalens, a maximum radius $r_{\max}$ can be determined by n_{eff}

$$\Delta n_{eff} = \frac{1}{h}\left(\sqrt{r_{\max}^2 + f^2} - f\right) \tag{12}$$

The values of n_{eff} for all considered atoms are bounded by the background material (air) and the chosen dielectric material (SiN). According to the n_{eff} distribution, they realized a transmission-mode achromatic metalens in the visible spectrum from 430 nm to 780 nm with focal length 81.5 μm and an experimental NA of 0.086, and the measured focusing efficiency can be maintained in the range of 36%–55%. Later, Wang et al. [27] realized a larger design freedom of GD by improving the fabrication limit and experimentally demonstrated an achromatic metalens based on a record-high aspect ratios fabrication. By increasing the height of TiO$_2$ atoms to 1500 nm, they achieved a larger GD (Eq. (11)) for achromatic design and overcame the low focusing efficiency at near-IR wavelengths (650 nm–1000 nm). A 25 μm diameter metalens is with NA = 0.1 and average focusing efficiency of 77.1%–88.5%. The high average focusing efficiency implies a possibility of practical application of achromatic metalenses in the future.

In 2018, Shrestha et al. [28] proposed an achromatic metalens design with a similar principle, by creating libraries of symmetric meta-atoms with various complex geometries. They described the modulation of meta-atoms by "phase-dispersion" space (shown in Fig. 4(a)) and concluded a design method of achromatic metalenses using the space. By choosing atoms with required values of dispersion at each position to fit GD profile, the chromatic aberration of metalenses can be controlled. As long as the range of phase at the selected wavelength covers 2π in the GD scale atoms have covered, there will always be suitable atoms for design. Similar to Eq. (12), Shrestha et al. also found that the range of phase dispersion ΔGD covered by the meta-atoms limits the maximum radius $r_{\max}$

$$r_{\max} \leq \frac{\Delta\text{GD} \cdot \text{c}}{\left(\dfrac{1}{\text{NA}} - \sqrt{\dfrac{1}{\text{NA}^2} - 1}\right)} \tag{13}$$

while

$$\Delta\text{GD} = \left(\max\left(\frac{\partial\varphi}{\partial\omega}\right) - \min\left(\frac{\partial\varphi}{\partial\omega}\right)\right) \tag{14}$$

They provided a metalens with polarization-independent focusing efficiencies up to 50% working in the transmission mode, which realized a near-constant focal length over $\lambda = 1200$–1650 nm. Also, concentrating on the degree of freedom of atoms' structure, Ndao et al. [29] demonstrated polarization-independent metalenses using a TiO$_2$ based fishnet-like structure with diameter of 20 μm shown in Fig. 4(b), which is also 90° spatial rotational symmetric. They experimentally reported an unchanged focal length when the wavelength varies from 640 nm to 1200 nm with a numerical aperture NA = 0.12 and measured average efficiencies over 70% in the continuous broadband.
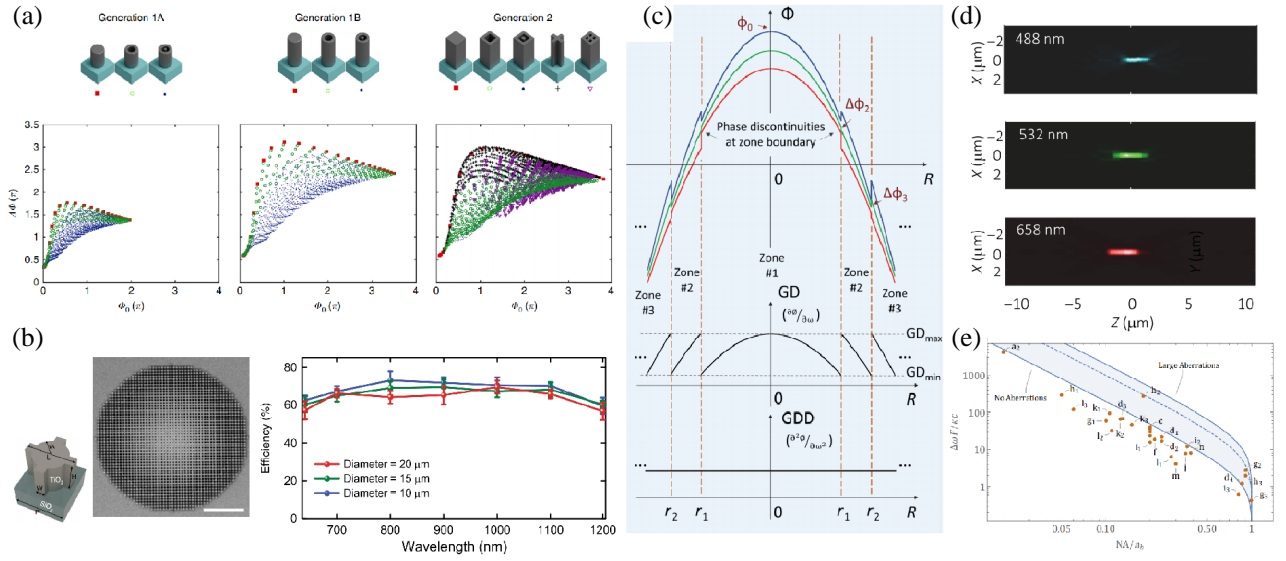
Figure 4. (a) Schematics of different meta-atoms [28], and their "phase-dispersion" space. (b) Fishnet atom metalens of diameter $20\,\mu\mathrm{m}$. Scale bar: $5\,\mu\mathrm{m}$. Focusing efficiency and the measured average efficiency is about 70% [29]. (c) Phase profile, the group delay (GD) profile, and the group delay dispersion (GDD) profile designed for a multi-zone, RGB-achromatic metalens [32]. The zone is defined by an area with continuously changed dispersion. Phase discontinuities at zone boundaries, zone transition locations, and initial phase at the lens centers require independent control. (d) Measured focal intensity distribution of the metalens [32]. (e) Limit based on Tucker's TBP (Time-bandwidth products) bound. Each data point in the plots represent a single design [34].

The methods mentioned above are all top-down design with a fixed period. The periodicity will encounter the accurate phase fit problem at the edge of a large metalens and necessarily entails large focusing efficiency losses. Chung et al. [30] proved this assumption and demonstrated an inverse design method breaking the periodicity of meta-units. They achieved an achromatic metalens from $\lambda = 450$–$700\,\mathrm{nm}$ with average focusing efficiency of 65%. Another advantage of inverse design is that it is based on full-wave simulations, which can accurately model the interactions between the atoms [31] and improve the focusing efficiency, which has a huge potential in the future metalenses' design.

Notice that all the design methods propose a limited relation that the range of the group delay $\Delta\mathrm{GD}$ determines the maximum radius of achromatic metalenses. Li et al. [32] in 2020 presented a general design principle to achieve large-area, multi-wavelength achromatic metalenses. They imitated the design principle of Fresnel lens of wrapping the phase profile at design wavelength from 0 to 2π in each zone. Instead of wrapping phase, they wrapped the GD profile from the minimum to the maximum boundary that is confined by the meta-atoms' library shown in Fig. 4(c). By this way, the maximum radius can be expanded to a much larger value. However, the fold of the GD profile imports an additional phase discontinuity $\Delta\varphi_i(\omega)$ on each zone's phase profile, where i represents the number of zones. By using a gradient-based optimization method [33], they optimized $\Delta\varphi_i$ to maximize the minimum value of the focusing intensity at design frequencies. So lights from different zones constructively interfere at a focal spot for all design frequencies, which represents the same focal length at different wavelengths. They achieved a 2-mm-diameter Red-Green-Blue (RGB) achromatic metalens (shown in Fig. 4(d)) by increasing the zone number and demonstrated the performance in a compact virtual reality (VR) platform.

Regardless of the design methods of these single metalens, the achromatic bandwidth and NA have a trade-off relationship. While a wide achromatic bandwidth has been achieved, the largest obtainable NA will be limited. Presutti and Monticone [34] derived fundamental bandwidth limits applicable to broadband achromatic metalenses. In any time-invariant system, the product between achievable time delay and bandwidth is limited by a dimensionless quantity κ, which always depends on some general

properties of the device, such as its length and refractive-index contrast of the materials involved. They discussed the expression of this value in three cases and gave the limit of bandwidth $\Delta\omega$ in each case.

1) For ultra-thin metasurfaces based on resonant meta-atoms (named Single Resonator)

$$\Delta\omega \leq \frac{2c}{f}\Theta\left(\frac{\text{NA}}{n_b}\right) \tag{15}$$

2) For waveguide-based dielectric metasurfaces (named Tucker)

$$\Delta\omega \leq \omega_c\frac{h\left(n_{\max} - n_b\right)}{f}\Theta\left(\frac{\text{NA}}{n_b}\right) \tag{16}$$

3) For generic metasurfaces (not necessarily dielectric and lossless) of thickness larger than the wavelength (named Miler)

$$\Delta\omega \leq \omega_c\frac{h\eta_{\max}}{f}\Theta\left(\frac{\text{NA}}{n_b}\right) \tag{17}$$

where h is the thickness of metalens; $\omega_c = 2\pi/\lambda_c$; λ_c is the band-center wavelength; and they replace

$$\Theta\left(\frac{\text{NA}}{n_b}\right) = \frac{\sqrt{1 - (\text{NA}/n_b)^2}}{1 - \sqrt{1 - (\text{NA}/n_b)^2}} \tag{18}$$

We can draw a conclusion from the formula that an effective way to realize a large NA, broadband achromatic metalens is to increase the meta-atoms height, which on the other hand is limited by fabrication technology. It is also worth to note that the above bandwidth limit is obtained when the additional phase provided by atoms satisfies the ideal achromatic phase distribution. It means that for metalenses that have not reached the diffraction limit, this bandwidth limit can be relaxed.

The design methods mentioned above can also be applied in other wavelengths, such as terahertz regime, which will expand the application to hyperspectral terahertz bio-imaging, spectroscopy, time-of-flight tomography, and other areas. In 2019, Cheng et al. [35] proposed an achromatic metalens in terahertz regime from 0.3 Thz to 0.8 THz (1 mm to 0.375 mm) with solid and inverse C-shaped atoms. Using silicon resonant atoms like the IRUEs methods, they achieved a metalens with diameter of 10 mm and NA = 0.385. Zhao et al. [36] demonstrated a terahertz achromatic metalens from 2.29 THz to 2.7 THz (0.13 mm to 0.11 mm) in 2020, and they controlled GD and phase respond of 20 different meta-atoms and optimized the metalens with a diameter of 10.22 mm and NA of 0.125.

As the frequency bandwidth of terahertz regime is much smaller than visible range, it is easier to fabricate a larger size of metalenses working in this regime and offers more opportunities to put into practical application.

2.2. Multi-Piece Achromatic Metalenses

The achromatic metalenses introduced above are all composed of single piece and have a theoretical limit of achromatic bandwidth and aperture size of different thicknesses. It is notable from Eq. (18) that the designable bandwidth can be expanded by increasing the thickness or length of devices. Consequently, there is another way to design achromatic metalenses by cascading multiple metalenses or combining with conventional lenses.

Chen et al. [37] in 2018 proposed a design of a meta-corrector for a commercial spherical lens. Considering the optical path in the glass L_1 and L_4 (shown in Fig. 5(a)), which can be obtained through commercial ray-tracing software such as Zemax OpticsStudio, they designed the meta-corrector with required phase profile given by:

$$\varphi\left(r, \omega_d\right) = n\frac{\omega_d}{c}\left[T_s - L_1(r)\right] + \frac{\omega_d}{c}\left[g + f - L_2(r) - L_4(r)\right] + n\frac{\omega_d}{c}\left[T - L_3(r)\right] \tag{19}$$

Subsequently, the required GD and GDD can be established as well. They took advantages of the coupled TiO_2 nanofins' dispersion by changing their geometric parameters. Such slot waveguide structures bring them a better dispersion control than single waveguides [38, 39]. These nanofins are arranged along $\pm 45°$ with respect to the x-axis so that the meta-corrector can correct aberrations for any
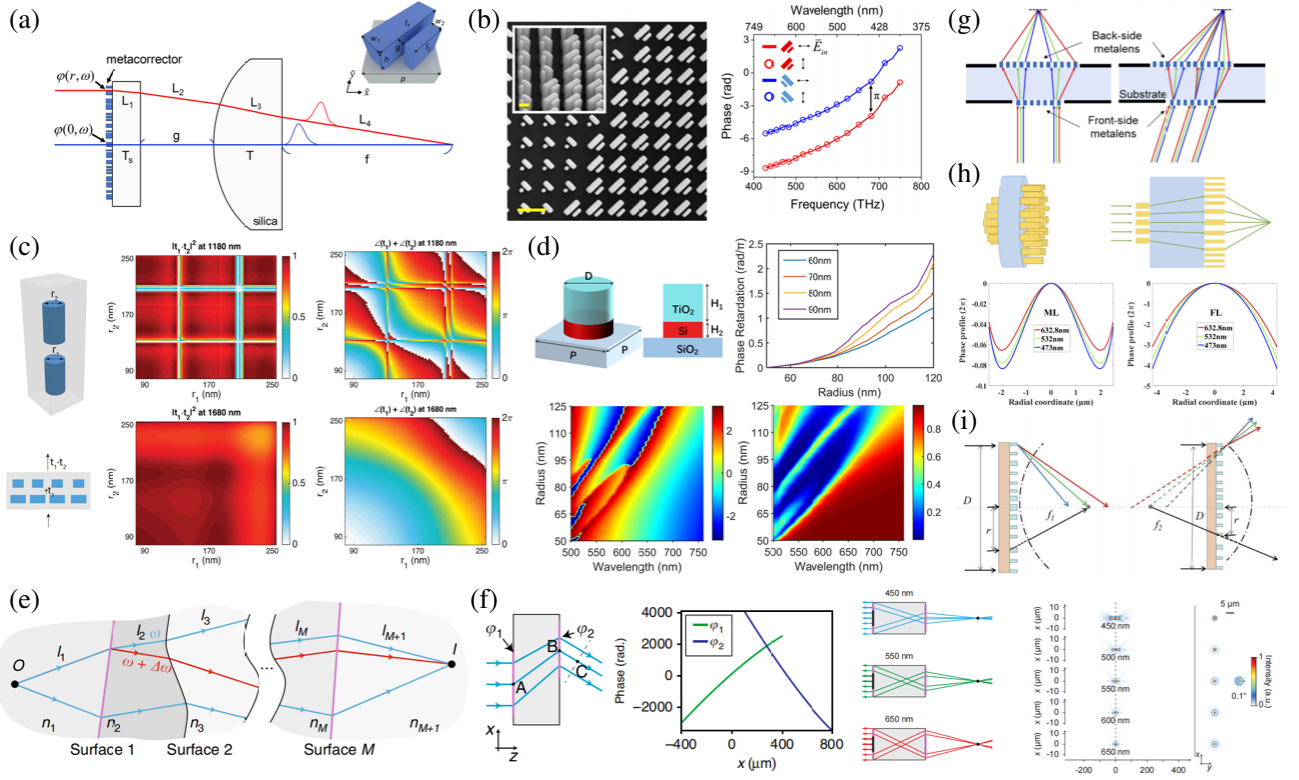
Figure 5. (a) Schematic of a hybrid lens consisting of a meta-corrector and a spherical lens [37]. (b) Scanning microscope image of the meta-corrector. Scale bar: 500 nm. Simulated phase shift. The incident polarization is x or y axises (depicted by black arrows in the legend) [37]. (c) Schematic of a doublet unit cell [43]. The overall transmission and phase maps. (d) Double-layer meta-atom structure composed of a poly-Si layer and a TiO$_2$ layer. Phase retardation function of the atom radius. Simulated phase and transmission maps, respectively [44]. (e) Rays (blue lines) travel from object point O through a system of M surfaces to image point I. Purple interfaces represent metasurfaces, and black interfaces represent boundaries [43]. (f) Schematic of an achromatic bilayer metasurface beam deflector and its phase profiles of the metasurfaces. Axial and transverse intensity distributions [45]. (g) Correction of both chromatic and monochromatic aberrations with the doublet metalens system [46]. (h) Schematic view of the doublet metalens. Ideal phase profile of the modulation layer (ML) and of the focusing layer (FL) [47]. (I) Schematics of the dual-layer achromatic metalens (DAML). Composed of a plano-convex liked metalens (PVML) and a plano-concave liked metalens [49].

incident polarization. This 90 degree rotation provided a π phase shift without changing the dispersion as shown in Fig. 5(b). It added a new degree of freedom to control phase and relaxed the phase coverage requirement to π. They successfully corrected spherical and chromatic aberrations of the commercial lens.

Recently, several other metalens doublets works have been proposed, such as multilayer metalens [40], wide field of view (FOV) doublet metalens [41], and orthogonal doublet metalens [42]. In 2018, Zhou et al. [43] proposed a method by employing tightly spaced multilayer dielectric metasurfaces shown in Fig. 4(c). They used vertically stacked Si meta-atoms embedded in PDMS and designed the distance between the atoms which are close enough to minimize wavefront divergence after the first layer, but far enough to avoid coupling. As a result, the overall phase and transmission can be calculated as the sum of the phase shift ($\angle t_1 + \angle t_2$) and product of the transmission ($|t_1 t_2|^2$). Because the radius of atoms at each layer can be varied individually, they obtained additional degrees of freedom to fit the multi-wavelength phase profile. To validate this approach experimentally, they designed and fabricated a metalens doublet that has a 500 μm diameter and a focal length of 600 μm (NA = 0.42) with

focusing efficiencies of 5.1% and 22% at wavelengths of 1180 nm and 1680 nm, respectively. However, the fabrication steps of this method are too complicated, and the fabrication error will unavoidably influence the performance of the metalens.

In 2021, Yao et al. [44] proposed a metalens composed of double-layer circular nanopillars constructed by poly-Si and TiO$_2$. Utilizing high refractive poly-Si and low absorptive TiO$_2$, the aspect ratio of this double-layer meta-atom can be reduced significantly. Considering the absorption of poly-Si, they reduced the height of the poly-Si layer to 80 nm and confirmed this idea by simulation. Their achromatic metalens had a stable focal length in the 620–675 nm wavelength range with the focusing efficiency exceeding 22%. This double layer design can be further optimized by controlling GD and GDD of each atom. However, fabricating the meta-atom with required aspect ratio will also remain challenging since the refractive index of TiO$_2$ is not large enough.

Experiences of the chromatic dispersion engineering method for conventional optical systems are also useful in achromatic metalenses design. McClung et al. [45] present a fundamental relation connecting an optical system's dispersion to the trajectories light through it as shown in Fig. 5(e). The system brings a set of rays of different frequencies ω from object point O to image point I. The accumulated phase of a fiducial ray can be expressed as

$$\varphi = \sum_{m=1}^{M+1} \frac{\omega}{c} n_m l_m + \sum_{m=1}^{M} \varphi_m \tag{20}$$

where l_m is the path length between surfaces $m-1$ and m inside a material with refractive index n_m, and φ_m is the phase imparted by the mth surface, which is provided by metasurface in this case. This system is achromatic only if $\Delta\varphi = l_g \Delta\omega/c$ is the same for all rays, so Eq. (20) can be rewritten as

$$l_g = \sum_{m=1}^{M+1} n_{m_g} l_m + \sum_{m=1}^{M} c \frac{\partial \varphi_m}{\partial \omega} \tag{21}$$

where $n_{m_g} = d(\omega n_m)/d\omega$ represents the group index for the mth material, and l_g represents optical group length (OGL). Unlike the other methods which scans the range of GD$_m$ ($\partial\varphi_m/\partial\omega \neq 0$) to realize same l_g at every position on metalens, they realized non-dispersive condition (GD$_{1+2} = \partial(\varphi_1 + \varphi_2)/\partial\omega = 0$) and fixed the value of OGL by deflecting incident rays at different points on the first surface with different angles to points on the second surface. Therefore, they designed an annular aperture (150 μm < r_1 < 300 μm) to avoid the influence of paraxial regions, which will involve a minimum OGL lower than designed value into the system. By directing light along predetermined trajectories and keeping the OGL stationary, they obtained an achromatic bandwidth from 450 nm to 650 nm shown in Fig. 5(f).

This combing design approach was also used by Kim et al. [46] in 2020. They designed a doublet metalens utilizing a multi-wavelength targeted single metalens on one side and a broadband geometric phase metalens on the other side of the substrate as shown in Fig. 5(g). Therefore, the former metalens corrects chromatic aberration of the latter one and achieve a FOV of 60° at three wavelengths (445 nm, 532 nm, and 660 nm) with NAs being 0.33, 0.38, and 0.47, respectively. The back focal length from the latter metalens and objective plane remains unchanged. However, the effective focal length is different because principal planes are shifting with wavelength, which exhibits as a lateral chromatic aberration in imaging plane. Later, Huang et al. [47] used a similar design method with FOV of 60° and increased the NA to 0.61. They designed the former metalens as a Schmidt plate to correct spherical aberration [48] as shown in Fig. 5(h). In this way, they achieved an achromatic doublet metalens in the visible light range of 470 nm to 650 nm with focusing efficiency over 50% at normal incident.

Conventional achromatic doublets with different Abbe numbers is another way to achieve achromatic metalenses. Li et al. [49] introduced an effective Abbe number and designed a dual-layer chromatic metalens that consisted of a plano-convex liked metalens (PVML) and a plano-concave liked metalens (PCML) as shown in Fig. 5(I). They defined the effective Abbe numbers of PVML and PCML as

$$V_1 = \frac{f_{1F} f_{1C}}{f_{1D}(f_{1C} - f_{1F})}, \quad V_2 = \frac{f_{2F} f_{2C}}{f_{2D}(f_{2C} - f_{2F})} \tag{22}$$

where D, F, and C represent three predetermined wavelengths (589.3 nm, 486.1 nm, and 656.3 nm for visible range). By the transformation of the focal length formula of the doublet lens, they simplified the dispersion as

$$\Delta' = \frac{1}{V_1}\frac{1}{f_1} + \frac{1}{V_2}\frac{1}{f_2} - d\left(\frac{1}{V_1}\frac{1}{f_1}\frac{1}{f_2} + \frac{1}{V_2}\frac{1}{f_1}\frac{1}{f_2}\right) \tag{23}$$

where d is the distance between PVML and PCML. By finding a pair of metalenses with V_1, f_1, V_2, f_2 from all possible cases of PCML and PVML to minimize the dispersion $|\Delta'|$, they demonstrated a doublet metalens with a focal length difference less than 1.5 μm over 36 μm focal length from 400 nm to 700 nm. This method compensates the dispersion by the reverse dispersion properties of PVML and PCML rather than the meta-atoms themselves. Theoretically, they can use arbitrary meta-atoms for metalens design without considering their phase dispersion.

3. CONCLUSION

The current metalens design methods mainly rely on forward methods. Based on these methods, we establish periodic atoms library first using simulation software such as Lumerical FDTD, and then manipulate the phase profiles, GD and GDD dispersion under different wavelengths by optimizing specific atoms structures. Although the forward approach does help to simplify the solution to the problem, it suffers from low fill factor since it lacks the ability to account for coupling effects between atoms. Some researchers expand the period by combining two or more units [50, 51] to take the coupling into consideration, but the design inevitably introduces higher order diffractions or sacrifices the space utilization, which usually lead to efficiency loss. On the other hand, the ideal exit plane fields are non-periodic over each unit and cannot be represented by periodic diffraction orders. To this end, the inverse design methods have been investigated to optimize specific metalens for chromatic aberration correction by many researchers and obtained good performance in experiments [30, 31, 52].

With chromatic aberration corrected, metalenses can have great potential. However, there are still lots of challenges in the design limitation, and some important issues need to be considered. Because fabrication limits the aspect ratio of meta-atoms, it constrains the time-bandwidth product and determines the designable achromatic bandwidth and aperture size physically. Researchers have proposed methods by increasing the length of optical system by cascading metalenses recently. Then, using multi-layer material or new high refractive index material [53, 54] may be a potential solution to achieve larger achromatic bandwidth. Taking advantages of the high refractive index and mature fabrication technology, silicon has become a promising material in metalens design. On the other hand, other off-axis aberrations [11], like coma, field curvature, and astigmatism, should also be taken into consideration, to achieve achromatic metalens with large FOV. By solving this series of problems, achromatic metalenses could be a promising candidate to be applied in wearable displays, mobile phone camera, micro display (AR, VR), and other compact optical devices.

ACKNOWLEDGMENT

REFERENCES

1. Yu, N., P. Genevet, M. A. Kats, F. Aieta, J.-P. Tetienne, F. Capasso, and Z. Gaburro, "Light propagation with phase discontinuities: Generalized laws of reflection and refraction," *Science*, Vol. 334, 333–337, 2011.
2. Aieta, F., P. Genevet, M. A. Kats, N. Yu, R. Blanchard, Z. Gaburro, and F. Capasso, "Aberration-free ultrathin flat lenses and axicons at telecom wavelengths based on plasmonic metasurfaces," *Nano Lett.*, Vol. 12, 4932–4936, 2012.

3. Khorasaninejad, M., F. Aieta, P. Kanhaiya, M. A. Kats, P. Genevet, D. Rousso, and F. Capasso, "Achromatic metasurface lens at telecommunication wavelengths," *Nano Lett.*, Vol. 15, 5358–5362, 2015.

4. Aieta, F., M. A. Kats, P. Genevet, and F. Capasso, "Multiwavelength achromatic metasurfaces by dispersive phase compensation," *Science*, Vol. 347, 1342–1345, 2015.

5. Lalanne, P. and P. Chavel, "Metalenses at visible wavelengths: Past, present, perspectives," *Laser Photonics Rev.*, Vol. 11, 2016.

6. Liang, H., Q. Lin, X. Xie, Q. Sun, Y. Wang, L. Zhou, L. Liu, X. Yu, J. Zhou, T. F. Krauss, and J. Li, "Ultrahigh numerical aperture metalens at visible wavelengths," *Nano Lett.*, Vol. 18, 4460–4466, 2018.

7. Huang, L., X. Chen, H. Mühlenbernd, H. Zhang, S. Chen, B. Bai, Q. Tan, G. Jin, K.-W. Cheah, C.-W. Qiu, J. Li, T. Zentgraf, and S. Zhang, "Three-dimensional optical holography using a plasmonic metasurface," *Nat. Commun.*, Vol. 4, 2808, 2013.

8. Faraji-Dana, M., E. Arbabi, A. Arbabi, S. M. Kamali, H. Kwon, and A. Faraon, "Compact folded metasurface spectrometer," *Nat. Commun.*, Vol. 9, 4196, 2018.

9. Tittl, A., A. Leitis, M. Liu, F. Yesilkoy, D.-Y. Choi, D. N. Neshev, Y. S. Kivshar, and H. Altug, "Imaging-based molecular barcoding with pixelated dielectric metasurfaces," *Science*, Vol. 360, 1105–1109, 2018.

10. Zhu, A. Y., W.-T. Chen, M. Khorasaninejad, J. Oh, A. Zaidi, I. Mishra, R. C. Devlin, and F. Capasso, "Ultra-compact visible chiral spectrometer with meta-lenses," *APL Photonics*, Vol. 2, 036103, 2017.

11. Aieta, F., P. Genevet, M. Kats, and F. Capasso, "Aberrations of flat lenses and aplanatic metasurfaces," *Opt. Express.*, Vol. 21, 31530–31539, 2013.

12. Millán, M. S., J. Otón, and E. Pérez-Cabré, "Chromatic compensation of programmable Fresnel lenses," *Opt. Express*, Vol. 14, 6226–6242, 2006.

13. Arbabi, E., A. Arbabi, S. M. Kamali, Y. Horie, and A. Faraon, "Multiwavelength metasurfaces through spatial multiplexing," *Sci. Rep.*, Vol. 6, 32803, 2016.

14. Hu, J., C.-H. Liu, X. Ren, L. J. Lauhon, and T. W. Odom, "Plasmonic lattice lenses for multiwavelength achromatic focusing," *ACS Nano.*, Vol. 10, 10275–10282, 2016.

15. Tang, F., X. Ye, Q. Li, Y. Wang, H. Yu, W. Wu, B. Li, and W. Zheng, "Dielectric metalenses at long-wave infrared wavelengths: Multiplexing and spectroscope," *Results Phys.*, Vol. 18, 103215, 2020.

16. Khorasaninejad, M., Z. Shi, A. Y. Zhu, W. T. Chen, V. Sanjeev, A. Zaidi, and F. Capasso, "Achromatic metalens over 60 nm bandwidth in the visible and metalens with reverse chromatic dispersion," *Nano Lett.*, Vol. 17, 1819–1824, 2017.

17. Arbabi, E., A. Arbabi, S. M. Kamali, Y. Horie, and A. Faraon, "Dispersionless metasurfaces using dispersive meta-atoms," *Conference on Lasers and Electro-Optics (CLEO)*, 1–2, 2016.

18. Wang, S., P. C. Wu, V.-C. Su, Y.-C. Lai, C. H. Chu, J.-W. Chen, S.-H. Lu, J. Chen, B. Xu, C.-H. Kuan, T. Li, S. Zhu, and D. P. Tsai, "Broadband achromatic optical metasurface devices," *Nat. Commun.*, Vol. 8, 187, 2017.

19. Berry, M. V., "Quantal phase factors accompanying adiabatic changes," *Proc. R. Soc. Lond.*, Vol. 392, 45–57, 1996.

20. Kanwal, S., J. Wen, B. Yu, D. Kumar, X. Chen, Y. Kang, C. Bai, and D. Zhang, "High-efficiency, broadband, near diffraction-limited, dielectric metalens in ultraviolet spectrum," *Nanomaterials*, Vol. 10, 2020.

21. Wang, S., P. C. Wu, V.-C. Su, Y.-C. Lai, M.-K. Chen, H. Y. Kuo, B. H. Chen, Y. H. Chen, T.-T. Huang, J.-H. Wang, R.-M. Lin, C.-H. Kuan, T. Li, Z. Wang, S. Zhu, and D. P. Tsai, "A broadband achromatic metalens in the visible," *Nat. Nanotechnol.*, Vol. 13, 227–232, 2018.

22. Chen, W. T., A. Y. Zhu, V. Sanjeev, M. Khorasaninejad, Z. Shi, E. Lee, and F. Capasso, "A broadband achromatic metalens for focusing and imaging in the visible," *Nat. Nanotechnol.*, Vol. 13, 220–226, 2018.

23. Khorasaninejad, M., A. Y. Zhu, C. Roques-Carmes,, W. T. Chen, J. Oh, I. Mishra, R. C. Devlin, and F. Capasso, "Polarization-insensitive metalenses at visible wavelengths," *Nano Lett.*, Vol. 16, 7229–7234, 2016.

24. Guo, Y., Z. Jafari, L. Xu, C. Bao, P. Liao, G. Li, A. Agarwal, L. Kimerling, J. Michel, A. Willner, and L. Zhang, "Ultra-flat dispersion in an integrated waveguide with five and six zero-dispersion wavelengths for mid-infrared photonics," *Photonics Res.*, Vol. 7, 1279, 2019.

25. Arbabi, E., A. Arbabi, S. M. Kamali, Y. Horie, and A. Faraon, "Controlling the sign of chromatic dispersion in diffractive optics with dielectric metasurfaces," *Optica*, Vol. 4, 625–632, 2017.

26. Fan, Z.-B., H.-Y. Qiu, H.-L. Zhang, X.-N. Pang, L.-D. Zhou, L. Liu, H. Ren, Q.-H. Wang, and J.-W. Dong, "A broadband achromatic metalens array for integral imaging in the visible," *Light Sci. Appl.*, Vol. 8, 67, 2019.

27. Wang, Y., Q. Chen, W. Yang, Z. Ji, L. Jin, X. Ma, Q. Song, A. Boltasseva, J. Han, V. M. Shalaev, and S. Xiao, "High-efficiency broadband achromatic metalens for near-IR biological imaging window," *Nat. Commun.*, Vol. 12, 5560, 2021.

28. Shrestha, S., A. C. Overvig, M. Lu, A. Stein, and N. Yu, "Broadband achromatic dielectric metalenses," *Light Sci. Appl.*, Vol. 7, 85, 2018.

29. Ndao, A., L. Hsu, J. Ha, J.-H. Park, C. Chang-Hasnain, and B. Kanté, "Octave bandwidth photonic fishnet-achromatic-metalens," *Nat. Commun.*, Vol. 11, 3205, 2020.

30. Chung, H., H. Chung, O. D. Miller, and O. D. Miller, "High-NA achromatic metalenses by inverse design," *Opt. Express*, Vol. 28, 6945–6965, 2020.

31. Zhou, M., D. Liu, S. W. Belling, H. Cheng, M. A. Kats, S. Fan, M. L. Povinelli, and Z. Yu, "Inverse design of metasurfaces based on coupled-mode theory and adjoint optimization," *ACS Photonics*, Vol. 8, 2265–2273, 2021.

32. Li, Z., P. Lin, Y.-W. Huang, J.-S. Park, W. T. Chen, Z. Shi, C.-W. Qiu, J.-X. Cheng, and F. Capasso, "Meta-optics achieves RGB-achromatic focusing for virtual reality," *Sci. Adv.*, Vol. 7, eabe4458, 2021.

33. Svanberg, K., "A class of globally convergent optimization methods based on conservative convex separable approximations," *SIAM J. Optim.*, Vol. 12, 555–573, 2002.

34. Presutti, F. and F. Monticone, "Focusing on bandwidth: Achromatic metalens limits," *Optica*, Vol. 7, 624, 2020.

35. Cheng, Q., M. Ma, D. Yu, Z. Shen, J. Xie, J. Wang, N. Xu, H. Guo, W. Hu, S. Wang, T. Li, and S. Zhuang, "Broadband achromatic metalens in terahertz regime," *Sci. Bull.*, Vol. 64, 1525–1531, 2019.

36. Zhao, F., Z. Li, X. Dai, X. Liao, S. Li, J. Cao, Z. Shang, Z. Zhang, G. Liang, G. Chen, H. Li, and Z. Wen, "Broadband achromatic sub-diffraction focusing by an amplitude-modulated terahertz metalens," *Adv. Opt. Mater.*, Vol. 8, 2000842, 2020.

37. Chen, W. T., A. Y. Zhu, J. Sisler, Y.-W. Huang, K. M. A. Yousef, E. Lee, C.-W. Qiu, and F. Capasso, "Broadband achromatic metasurface-refractive optics," *Nano Lett.*, Vol. 18, 7801–7808, 2018.

38. Tong, L., J. Lou, and E. Mazur, "Single-mode guiding properties of subwavelength-diameter silica and silicon wire waveguides," *Opt. Express*, Vol. 12, 1025, 2004.

39. Almeida, V. R., Q. Xu, C. A. Barrios, and M. Lipson, "Guiding and confining light in void nanostructure," *Opt. Lett.*, Vol. 29, 1209, 2004.

40. Saeidi, C. and D. van der Weide, "Wideband plasmonic focusing metasurfaces," *Appl. Phys. Lett.*, Vol. 105, 053107, 2014.

41. Groever, B., W. T. Chen, and F. Capasso, "Meta-lens doublet in the visible region," *Nano Lett.*, Vol. 17, 4902–4907, 2017.

42. Shi, X., D. Meng, Z. Qin, Q. He, S. Sun, L. Zhou, D. R. Smith, Q. H. Liu, T. Bourouina, and Z. Liang, "All-dielectric orthogonal doublet cylindrical metalens in long-wave infrared regions," *Opt. Express*, Vol. 29, 3524–3532, 2021.

43. Zhou, Y., I. I. Kravchenko, H. Wang, J. R. Nolen, G. Gu, and J. G. Valentine, "Multilayer non-interacting dielectric metasurfaces for multiwavelength metaoptics," *Nano Lett.*, Vol. 18, No. 12, 7529–7537, 2018.

44. Yao, Z., W. Chen, and Y. Chen, "Double-layer metalens with a reduced meta-atom aspect ratio," *Opt. Lett.*, Vol. 46, 1510–1513, 2021.

45. McClung, A., M. Mansouree, and A. Arbabi, "At-will chromatic dispersion by prescribing light trajectories with cascaded metasurfaces," *Light Sci. Appl.*, Vol. 9, 93, 2020.

46. Kim, C., S.-J. Kim, and B. Lee, "Doublet metalens design for high numerical aperture and simultaneous correction of chromatic and monochromatic aberrations," *Opt. Express*, Vol. 28, 18059–18076, 2020.

47. Huang, Z., M. Qin, X. Guo, C. Yang, and S. Li, "Achromatic and wide-field metalens in the visible region," *Opt. Express*, Vol. 29, 13542–13551, 2021.

48. Johnson, T. J. and J. F. O'rourke, "Method for making replica contour block masters for producing Schmidt corrector plates," U.S. patent US3837124 A, 1974.

49. Li, M., S. Li, L. K. Chin, Y. Yu, D. P. Tsai, and R. Chen, "Dual-layer achromatic metalens design with an effective Abbe number," *Opt. Express*, Vol. 28, 26041–26055, 2020.

50. Khorasaninejad, M., W. T. Chen, A. Y. Zhu, J. Oh, R. C. Devlin, C. Roques-Carmes, I. Mishra, and F. Capasso, "Visible wavelength planar metalenses based on titanium dioxide," *IEEE J. Sel. Top. Quantum Electron.*, Vol. 23, 43–58, 2017.

51. Spägele, C., M. Tamagnone, D. Kazakov, M. Ossiander, M. Piccardo, and F. Capasso, "Multifunctional wide-angle optics and lasing based on supercell metasurfaces," *Nat. Commun.*, Vol. 12, 3787, 2021.

52. Elsawy, M. M. R., A. Gourdin, M. Binois, R. Duvigneau, D. Felbacq, S. Khadir, P. Genevet, and S. Lanteri, "Multiobjective statistical learning optimization of RGB metalens," *ACS Photonics*, Vol. 8, 2498–2508, 2021.

53. Yoon, G., K. Kim, D. Huh, H. Lee, and J. Rho, "Single-step manufacturing of hierarchical dielectric metalens in the visible," *Nat. Commun.*, Vol. 11, 2268, 2020.

54. Li, N., Z. Xu, Y. Dong, T. Hu, Q. Zhong, Y. H. Fu, S. Zhu, and N. Singh, "Large-area metasurface on CMOS-compatible fabrication platform: Driving flat optics from lab to fab," *Nanophotonics*, Vol. 9, No. 10, 3071–3087, 2020.